Geometric Optimization Algorithm for Path Loss Model of Riparian Zone IoT Networks Based on Federated Learning Framework

Yu Geng[1,2], Tiecheng Song[1*], Qiang Wang[2], and Xiaoqin Song[3]
[1] National Mobile Communication Research Lab, Southeast University
Nanjing 210096, China
[e-mail: yugeng93@gmail.com]
[2] China Information Consulting & Designing Institute (CICDI) CO., LTD.
Nanjing 210000, China
[3] College of Electronic and Information Engineering, Nanjing University of Aeronautics and Astronautics
Nanjing 211106, China
*Corresponding author: Tiecheng Song

Abstract

In the field of environmental sensing, it is necessary to develop radio planning techniques for the next generation Internet of Things (IoT) networks over mixed terrains. Such techniques are needed for smart remote monitoring of utility supplies, with links situated close to but out of range of cellular networks. In this paper, a three-dimension (3-D) geometric optimization algorithm is proposed, considering the positions of edge IoT devices and antenna coupling factors. Firstly, a multi-level single linkage (MLSL) iteration method, based on geometric objectives, is derived to evaluate the data rates over ISM 915 MHz channels, utilizing optimized power-distance profiles of continuous waves. Subsequently, a federated learning (FL) data selection algorithm is designed based on the 3-D geometric positions. Finally, a measurement example is taken in a meadow biome of the Mexican Colima district, which is prone to fluvial floods. The empirical path loss model has been enhanced, demonstrating the accuracy of the proposed optimization algorithm as well as the possibility of further prediction work.

1. Introduction

The development of the Internet of Things (IoT) has a tendency to expand to the edge [1]. The transmission environment of edge terminals has become more complex. High frequency technologies have led to more factors that can interfere with short-distance signal transmission [2]. Considering general IoT terminals' energy consumption and signal bandwidth, accurate calculation of transmission path loss in new application scenarios is the guarantee for edge system networking operation [3].

A common solution is the use of empirical models. The derivation of an empirical model is often challenged by large-scale measurement campaigns. Propagation measurements sounder system often assume a single transmitter and a few fix receivers. Hence, large-scale IoT models usually present fixed values of the parameters (e.g., [4] – [6]). However, the above assumption may be unrealistic in short-range rural IoT scenarios, since such IoT edge systems may be closed to the ground. The propagation system suffers from ground reflection, absorption, and vegetation attenuation [7]. The heterogeneous obstacles in the catchment area may affect different measurement point. General empirical model would imply similar PL characteristics for all environment in the same distance [8]. The propagation studies summarized in this paper aim to serve rural short-range IoT edge network. As an extended tentacle of existing mobile edge computing (MEC) system, the terminal devices' location environment usually be harsh. Especially for those emergences warning system.

For the topographical scenarios of the form encountered in riparian zones, various propagation models have been muted, some based on empirical methods others on physical optics. However, the aforementioned test strategy encountered one unforeseen complication, with measurement positions being forced to deviate from the intended LOS axis between transmitter and receiver due to man-made & natural obstructions. This introduced unquantified fluctuations in the propagation path ERP as the angle between the transmit & receive antenna bore-sight orientations varied in both azimuth and elevation with each measurement position. Furthermore, variations in ground moisture content and permittivity due to the enhanced deviation of the test position from this originally intended transmitter/receiver antenna straight line axis presented another potential unknown.

In order to derive the optimum fit to this original data set, a geometrically customized enhanced two-ray path model was formulated to emulate the results [9]. The ensuing optimization process comprised the minimization of an objective function including three of the model parameters namely, the transmission ERP and ground complex permittivity real and imaginary parts. The multi-level single linkage (MLSL) inversion technique used for this optimization is particularly adept at multi-parameter minimization problems and has been successfully applied for the near-field propagation inversion application detailed in [10].

However, the optimized one empirical path loss model still affected by the uncorrelated data. To increase the model accuracy, the author intends to establish an objective-based federated learning algorithm according to the novel geometric parameters obtained in the paper. FL is an emerging technology with privacy protection in AI [11]. It takes advantage of distributed data sources by building a machine learning model. The FedAvg [12] aggregation method has been widely used under the assumption of the independent and identically distributed (IID) data pattern. Nonetheless, data heterogeneity poses undesired challenges [13]. Specifically, an IoT network usually consists of devices that differ in energy consumption level, communication network condition, data computation capability. Therefore, clients can collect unbalanced and dissimilar data sets due to the diverse environments.

As the non-independent and identical distribution (non-IID) manner data sets are

statistically different from each other, it is difficult to employ the linear-based FedAvg approach to obtain a globally optimized model. Likewise, Zhao et al. [14] showed that the accuracy of federated learning under the non-IID data set scenario can decrease by as much as 55%. Therefore, it is in dire need to address the non-IID federated learning problem in IoT networks. Normally, objective correlations need to be justified with different algorithm. Since we have given novel geometric objectives, which affect the path loss directly. Thus, in this paper, we design a novel propagation regulation algorithm to distribute the data. The key findings of this paper may be summarized as follows:

1) Spatial variations in the received signal strength (RSS) vs distance measurement test points may be measured and applied to a 3-D coordinate representation so that an accurate 2-ray path propagation model be formulated in terms of measurement angle dependent Tx/Rx coupling factors and ground inclination to the horizontal. Furthermore, coupling factor compensation may be applied to simulate and correct for bore-sight misalignment of the transmit and receive antennas (i.e., Gain compensation correction) so that simple n^{th} order polynomial models may be applied to the original data assuming spatial uniformity of ground complex permittivity applies.

2) A geometric objective based federated learning algorithm is designed for IoT edge network propagation model. By selecting different data into the cluster, proper MLSL iteration model can be calculation for the specific site condition. The algorithm aims for less computation while higher model accuracy by sort data and model in different groups.

3) A case study of the Colima riparian zone is studied. The method is proved optimal compared to the real measurement results as well as the empirical model obtained considering the entirely data. The method indicates a path loss prediction and new IoT device implement function.

The organization of this paper is as follows. section II introduces related work. In section III, the enhanced 2-ray model is derived for IoT environment. Optimized MLSL algorithm and geometric-objective based FL framework is presented in section IV to fit the measurement data as well as further path loss prediction. A riparian zone empirical case is analyzed in section V and conclusions are drawn in section VI.

2. Related Work

2.1 IoT Edge Network Propagation Model

A thorough search of the literature reveals an inadequacy of studies or data that analyze and design signal propagation models to support practical IoT deployment for different edge network environments. In recent research [15], intelligent reflecting surface (IRS) assisted IoT network is researched to extend the coverage area. The direction of the antenna is a key point of IRS performance. However, the end node (EN)'s location error is not classified. The study in [16] shows the improvement and advantage of using the low power tiny devices in term of node placement, orientation, and parameter considerations such as packet drop rate, signal-to-noise ratio (SNR), and node standalone energy source. Paper [5] introduces a LoRa signal two ray model fitting tidal waters environment. Tidal water may change the reflection point. But large-scale fade over water is researched in the article, of which positioning affects little towards the loss model. The study in [17] reveals gaps in research to analyze and design empirical propagation models to support large-scale stochastic implementations of wireless sensor network (WSN) in farm environment. Some research has been carried out but does not consider the actual sensing device suitable for the farm monitoring infrastructure. They do not

consider the excess attenuation of the signal due to changes in the crop's physical properties.

Most of the studies done on this subject are based on lab simulations of short-range rural areas using artificial databases and Monte Carlos simulations. Each determined factor is quantified and its respective impact mitigated through a two-sided approach: a set of correction mechanisms, and a specific measuring procedure aimed at effectively limiting the influence of such factors. Different IoT edge environment would be affected by the local factors. Signal positioning as well as 3-D geometric objectives have great influence on the ground level propagation loss. Furthermore, the exceed loss occurs due to the environment. For short range propagation model, this various exceed loss would affect the path loss. However, little recent research distinguishes the exceed loss exponent separately.

2.2 Federated learning in IoT networks

The federated learning is discussed in [18] for user input recommendation in mobile networks. For aggregation, [19] proposed the FedAvg approach under the assumption of the IID data sets over clients. In recent research [20], efficiency optimization strategies are proposed for the federated learning model, but they all consider the IID data set scenarios. Nonetheless, the heterogeneity of IoT systems results in the non-IID patterns that affect convergence performance, which has not been sufficiently addressed [21]. Moreover, several works have introduced solutions for federated learning with heterogeneity [22], [23]. In [22], the proposed approach generated a data set at the server for pre-training, and the data set is shared with clients to reduce the non-IID impacts. Nonetheless, the data exchange can pose extra communication overhead, heavy for IoT sensor networks with limited resources. Li et al. [23] proposed FedProx, a variation of the FedAvg, with an added proximal term to the aggregation for heterogeneous data sets. It intended to learn a single globally optimized model for all participating nodes.

In IoT networks, training separate models that better fit diverse distributions can improve the performance for specific data patterns for clients that collect data of the same model. Federated learning is a promising approach for IoT networks, especially when data privacy, bandwidth limitations, and edge computing capabilities are critical consideration. Implementing federated learning requires careful planning, model management, and security measures to ensure its effectiveness and security in IoT applications.

3. Enhanced Propagation Model

In this section, a propagation model is formulated linking to the salient propagation parameters, (i.e., path geometry, antenna gain and ground reflection coefficient), in order to yield the optimal correlation with the measured RSS data set. The model exploits the 3-D cylindrical coordinate position data to create a Cartesian representation of the measurement geometry with all way points assigned bespoke x, y, z coordinates. Expressing the position information in this manner enabled subtle changes in direct and reflected path vectors & ground reflection angles to be incorporated along with off bore-sight fluctuations in the Tx/Rx antenna gains (and coupled ERP's) on the propagation path. The method chosen for deriving these position coordinates is now described.

3.1 Gain Correction for Off Bore-sight Measurements

The schematic of **Fig. 1** provides the 3-D representation of the experimental set-up comprising two antennas of height h_T and h_R coupled on a sloping ground plane of inclination α - via direct and reflected path lengths R_D and R_R. This 3-D schematic illustrates how the 2-

ray propagation path lengths and incident angles may be derived via a consideration of the receive antenna image location in the ground plane. It also shows how for each way-point, with Cartesian coordinates x_n, y_n, z_n, and polar coordinates R_D, θ, ϕ, the propagation path vectors in conjunction with subtending angles ϕ, δ, θ, ξ & v, are instrumental in the determination of the antenna coupled directivity, spreading loss and ground plane reflection coefficient. The original measurement coordinates along with their Cartesian counterparts are provided in Section V below. From a study of the original polar coordinates illustrated in **Fig. 1**, it is evident that the relative height of the receive antenna base (at ground depression Δh) and associated tilt angle α with respect to the origin are given by:

$$\Delta h = H - H(0) \, ; \, \alpha = tan^{-1}(\Delta h/D_0) \tag{1}$$

Where H and is the height *a.s.l* of each measurement waypoint and $H(0)$ is the height *a.s.l* of the zeroth way point at the system origin (i.e., 0,0,0). The vector length D_0, between the origin and antenna base at each waypoint is therefore given by:

$$D_0 = \sqrt{(R_D)^2 - (h_T - h_R + \Delta h)^2} \tag{2}$$

and the angle between the horizontal and direct ray vectors linking the Tx and Rx antenna phase centers is given by:

$$\theta = tan^{-1}[(h_T - h_R + D_0 tan(\alpha))/D_0] \tag{3}$$

Finally, the coordinates of the individual measurement points may be computed thus:

$$x_n = D_0 \cos(\phi) \, ; \, y_n = D_0 \, sin(\phi) \, ; \, z_n = h_T - D_0 \tan(\theta) \tag{4}$$

From the above coordinate parameters, it's now possible to derive the other angles required to formulate the 2-ray path model for each individual point.
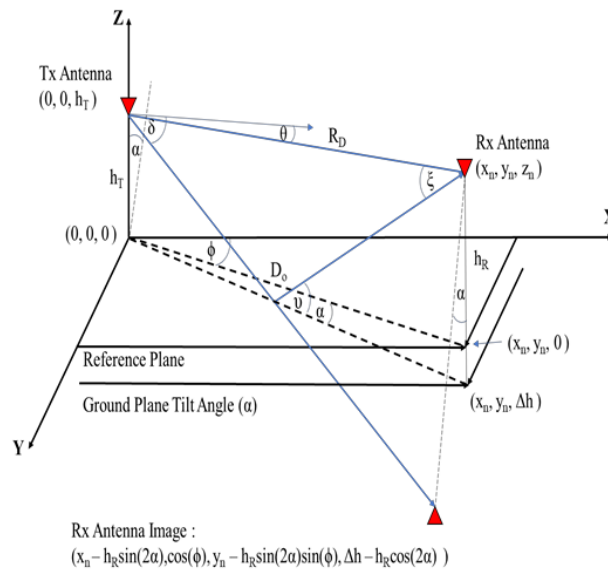
Fig. 1. Received signal strength (RSS) vs Distance Measurements: 3-D Cartesian Coordinate representation of measurement way-point locations displayed in aerial view of test region.

The angle between horizontal and ground reflected ray path is given by:

$$\delta = tan^{-1}([h_T + h_R \cos(2\alpha) + D_0\, tan(\alpha)]/D_0) \tag{5}$$

whilst the incident/reflected ray angle at the ground υ and receive antenna angles ξ are given by:

$$\upsilon = \delta - \alpha; \ \xi = \delta - 2\alpha \tag{6}$$

and the direct and reflected ray path lengths for the sloping slope angle α are given by:

$$R_D = \sqrt{(h_T - h_R + D_0 \tan(\alpha))^2 + (D_0)^2} \tag{7}$$

$$R_R = \sqrt{(h_T + h_R \cos(2\alpha) + D_0 \tan(\alpha))^2 + (D_0 - h_R \sin(2\alpha))^2} \tag{8}$$

3.2 The Enhanced 2-ray Propagation Model

The derivation of the direct & reflected path geometry described above, is key to the creation of a 'flat earth', 2-ray propagation model for each measurement waypoint. Ultimately the model, for a particular propagation constant and frequency of operation, facilitates mapping of the channel RF characteristics, i.e., the reflected ray amplitude and phase, the location of the multipath nulls and the juxtaposition between the Friis dominated $1/d^2$ propagation and $1/d^4$ ground wave attenuated regions (located at ~ 140 m for 915 MHz measurement case). Furthermore, the angular deviation of direct and reflected rays from antenna boresight as dictated by i.e., θ, δ, ξ & ϕ in **Fig. 1**, coupled with the antenna *E & H* radiation patterns, enables the variation of transmit and receive gains to be quantified along with the effective antenna coupled ERP for each test position. **Fig. 2** & **Fig. 3** in providing the elevation and plan geometry of a given nth measurement point, show how the antenna directivity will impact upon the coupled gain and propagation path ERP due to deviations of a given path from boresight. A study of the figures also shows how both Tx & Rx antennas exhibit the different Gain characteristics (one is a log periodic antenna the other a stacked dipole array), and why this difference should be accounted for in any rigorous formulation of the 2-ray path characteristics. The closed form solution for this 2-ray path model is now described.
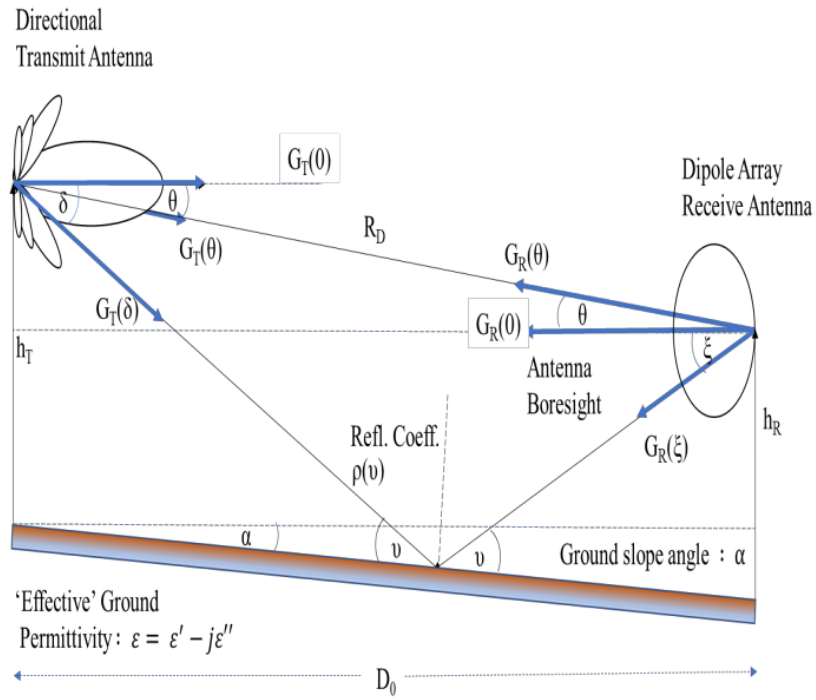
Fig. 2. 2-D elevation view of propagation path geometry for RSS vs distance measurements showing
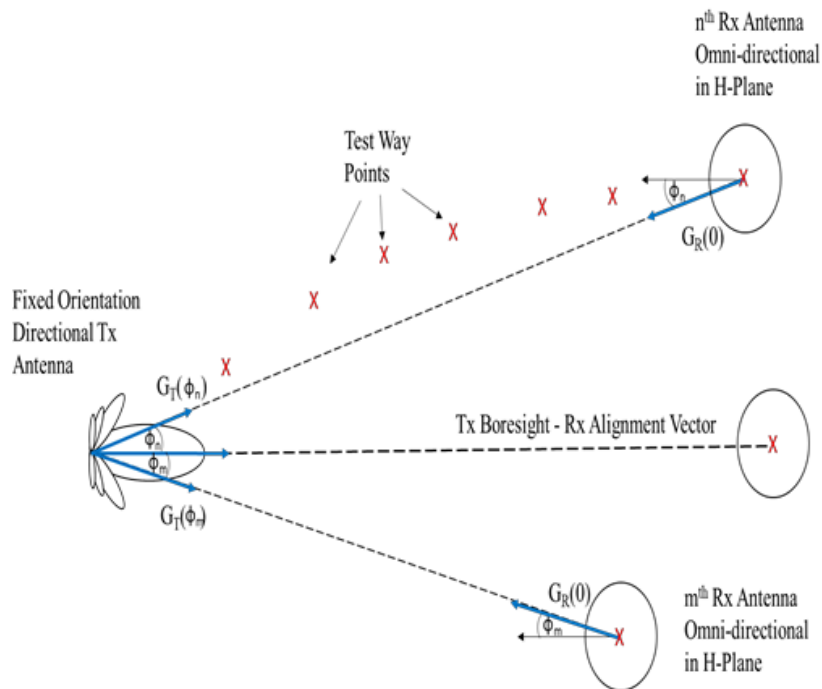direct & reflected path lengths & elevation angles in plane of vector D_0 in **Fig. 1**.

Fig. 3. 2-D plan view of propagation path geometry for RSS vs distance measurements showing
direct path lengths & azimuth angles in **Fig. 1**, along with antenna azimuthal gain deviation $G_T(\phi)$
due to Tx and Rx antenna bore-sight misalignment

A study of the elevation schematic in **Fig. 2**, shows how the received signal strength (referred to as the forward solution in the optimization process defined below), is derived via the summation of the direct and reflected vectors at a given waypoint to yield the resultant complex received *E-field* as:

$$E_T = \frac{E_0\sqrt{G_T(\theta,\phi)G_R(\theta,\phi)}e^{j\beta R_D}}{R_D} + \frac{\rho(\upsilon)E_0\sqrt{G_T(\delta,\phi)G_R(\xi,\phi)}e^{j\beta R_R}}{R_R} \qquad (9)$$

where the total received power within the free space propagation medium of intrinsic impedance η_0 is given by:

$$P_R = \frac{|E_T \cdot E_T^*|}{\eta_0} = \frac{P_T G_A G_T(\theta,\phi)G_R(\theta,\phi)\lambda^2}{(4\pi R_D)^2 L} \times \left|1 + \rho(\upsilon)\left(\frac{R_D}{R_R}\right)\sqrt{\frac{G_T(\delta,\phi)G_R(\xi,\phi)}{G_T(\theta,\phi)G_R(\theta,\phi)}}e^{j\gamma}\right|^2 \quad (10)$$

whilst the terms E_0 & γ are defined as:

$$E_0 = \sqrt{\frac{P_T G_A \eta_0}{T}}\left(\frac{\lambda}{4\pi}\right); \; \gamma = \beta(R_D - R_R) \qquad (11)$$

3.3 Geometric-related Coefficient and Approximation

3.3.1 Ground Reflection Coefficient

The standard form of the reflection coefficient for vertically polarized incidence irradiation used in these measurements and cited in (10) above is defined as:

$$\rho(\upsilon) = \frac{(\varepsilon' - j\varepsilon'')sin(\upsilon) - \sqrt{(\varepsilon' - j\varepsilon'') - cos^2(\upsilon)}}{(\varepsilon' - j\varepsilon'')sin(\upsilon) + \sqrt{(\varepsilon' - j\varepsilon'') - cos^2(\upsilon)}} \qquad (12)$$

where υ is the incidence angle as illustrated in **Fig. 2**. For the test region ambient ground conditions @ 915 MHz, the moisture dependent permittivity real parts and ground conductivity were found to be in the region of ε' = 5; σ = 0.03 S/m, a result which provided a close correlation with the optimization estimate detailed in section IV.

3.3.2 Antenna Gain Approximations and Coupling Factors

In order to define the 2-ray path model in terms of the transmit & receive antenna boresight gains and directivity dependent coupling factors, an *E* and *H-plane* aperture-based transformation approximation was applied. Here we assume the antenna pattern directivities specified above, may be approximated using assume a classic 'sinc-squared' functional dependence [24] in both θ and ϕ dependent planes, i.e., for the transmit antenna:

$$G_T(\theta,\phi) = G_T(0,0)sinc(\beta L_T^\upsilon sin(\theta))^2 sinc(\beta L_T^h sin(\phi))^2 \qquad (13)$$

where (L_T^v, L_T^h) are the transmit antenna vertical (*E-plane*) and horizontal (*H-plane*) equivalent aperture widths, whilst the Rx antenna aperture widths (L_R^v, L_R^h) and gain $G_R(\theta, \phi)$ assume similar forms. Substituting these Tx & Rx gain formulations into the received power profile function of (10) above and regrouping terms yields:

$$P_R = \frac{P_T G_A G_T(0,0) G_R(0,0) D_D(\theta, \phi) \lambda^2}{(4\pi R_D)^2 L} \times \left| 1 + \rho(v) \left(\frac{R_D}{R_R}\right) \sqrt{\frac{D_R(\delta, \xi, \phi)}{D_D(\theta, \phi)}} e^{j\gamma} \right|^2 \quad (14)$$

where the direct ray maximum gain normalised coupling factor between Tx & Rx may be described as:

$$D_D(\theta, \phi) = \left[\frac{G_T(\theta, \phi) G_R(\theta, \phi)}{G_T(0,0) G_R(0,0)} \right] =$$
$$[sinc(\beta L_T^v sin(\theta)) sinc(\beta L_T^h sin(\phi)) sinc(\beta L_R^v sin(\theta))]^2 \quad (15)$$

$$D_D(\delta, \xi, \phi) = \left[\frac{G_T(\delta, \phi) G_R(\xi, \phi)}{G_T(0,0) G_R(0,0)} \right] =$$
$$[sinc(\beta L_T^v sin(\delta)) sinc(\beta L_T^h sin(\phi)) sinc(\beta L_R^v sin(\xi))]^2 \quad (16)$$

Note as the receive antenna is omni-directional in the azimuthal or *H-plane* then $sinc(\beta L_R^h sin(\phi))^2 = 1$ for all ϕ, hence the omission of this term in equations (15) & (16).

3.3.3 Near/Far Field Approximations

It is now possible to obtain approximations for the received *1/d²* propagation region within the first Fresnel zone or 'critical distance' [24] and 4th power decay region beyond this point (i.e., ~ 140 to 1000 m in this particular 915 MHz measurement case). Within the first Fresnel zone an oscillatory propagation region exists, the approximate 'mean' of which can be described in terms of the direct path only. This term may be normalized to the direct path coupling formulation of (15) to yield a dependence attributable to the maximum ERP, distance and wavelength only,

$$P_C^{NF} = \frac{P_R}{D_D(\theta, \phi)} \approx \frac{P_T G_A G_T(0,0) G_R(0,0) \lambda^2}{(4\pi R_D)^2 L} \quad (17)$$

Similarly, in the far field region beyond the critical distance, the path model assumes a $1/(R_D)^4$ form as the oscillatory bracketed term in (14), (which reflects the interaction between direct and ground reflected rays), reduces to a basic sinusoidal dependence. Application of the approximations expressed in (18) below, along with coupling factor normalization as per (16) yields the following approximation for the far field Rx power:

$$\rho(v) \left(\frac{R_D}{R_R}\right) \sqrt{\frac{D_R(\delta, \xi, \phi)}{D_D(\theta, \phi)}} \approx 1; \quad \gamma = \frac{4\pi h_T h_R}{\lambda D_0}; \quad R_D \approx R_R \approx D_0$$
$$P_C^{FF} \approx \frac{P_T G_A G_T(0,0) G_R(0,0) (h_T h_R)^2}{(D_0)^4 L} \quad (18)$$

These approximations will be utilised in the curve fitting analysis describe later in greater detail in section IV.

4. Propagation Model Optimizations and Federated Learning Framework

4.1 Antenna Coupling Factors Estimations and Normalization

Knowledge of the Tx-Rx antenna 3-D radiation patterns is required for any estimation of the direct or reflected path directivities and mutual coupling factors (15,16). However, for the antennas used in these measurements, the bespoke 3-D Gain patterns were not provided by the manufacturer and only the azimuth & elevation principal plane 3 dB beamwidths were available. To resolve this, an inversion technique was applied to derive the effective *E & H-plane* aperture dimensions, simulate the elliptical 3-D antenna patterns and estimate the direct and reflected path directivities at each measurement point from the beamwidths alone. For this purpose, the transmit antenna aperture dimensions (L_R^v, L_R^h) were estimated from the *E & H-plane* beamwidths via derivation of the roots of the function:

$$sinc[\beta L_T^v sin(\varphi_{3dB})]^2 = 0.5; \; sinc[\beta L_T^H sin(\vartheta_{3dB})]^2 = 0.5 \tag{19}$$

The derivation of the antenna aperture widths in Section A now enables the direct and reflected path coupling factors to be computed via substitution of L_T^v, L_T^h & L_R^v into (15) & (16). These coupling functions are basically the product of the normalized antenna directivities for the Tx & Rx incidence angles with respect to boresight, i.e., δ, θ, ξ in **Fig. 3**. The direct path coupling factor $D_D(\theta, \phi)$ as defined in (14), has been interpolated as a function of distance R_D along with the corresponding discrete measurement values (denoted by an 'x'). A study of which shows that deviations of up to 4 dB from the maximum boresight coupling factor are in evidence. Note, the plot also shows the variation in Tx azimuthal angle ϕ in interpolated continuous form with distance for reference purposes.

In summary, the above analysis emphasizes the importance of accurate Tx-Rx path spatial monitoring and coupling normalization in any 2-ray path model, particularly when using highly directional antennas, as these will be more susceptible to boresight misalignment errors.

4.2 Optimization Curve Fitting for Two Ray Path Model

In this section, a novel MLSL inversion technique [25] was applied to search for the combination of model parameter values which provided the optimum correlation with the RSS vs distance data. This MLSL algorithm, which is particularly effective at finding the global minima for complex multi-parameter inversion problems, comprised three sections namely: the forward solution or objective function, the RMS error function and the optimization algorithm itself. The forward solution is effectively the enhanced two-ray path model (20), whilst the RMS error function is the 'least squares' difference between the synthetically generated forward solution and the measured data over all N points. The optimization algorithm extracts the objective function global minima from the myriad of local minima formed within the N parameter space. The (N=3) optimization variables in this instance being the total transmitter-receiver maximum coupled ERP and real and imaginary parts of the ground plane complex permittivity. The feasible range limits over which these variables were optimized are provided in **Table 1** below.

Table 1. Feasible range limits and start value used for MLSL inversion analysis

Parameter	Range lower limit	Range upper limit	Optimization start value
Tx-Rx ERP (mW)	500	2000	1000
Permittivity Real Part	1	10	5
Permittivity Imaginary Part	0	1	0.5

The propagation model forward solution was randomly varied to derive the set of parameters providing the optimum fit to the complete 915 MHz RSS data set. The forward solution is effectively the total received power (as defined previously in (11)) which may be re-expressed in terms of the 3 optimization variables, i.e., the maximum coupled ERP and the complex permittivity real and imaginary parts$(\varepsilon', \varepsilon'')$ for each nth measurement position as:

$$P_n(A_0, \varepsilon', \varepsilon'') = \frac{A_0 D_D(\theta, \phi)\lambda^2}{(4\pi R_D^n)^2} \left| 1 + \rho_n(v_n, \varepsilon', \varepsilon'') \left(\frac{R_D^n}{R_R^n}\right) \sqrt{\frac{D_R^n(\delta, \xi, \phi)}{D_D^n(\theta, \phi)}} e^{j\gamma n} \right|^2 \qquad (20)$$

where A_0 maximum coupled ERP is defined as:

$$A_0 = \frac{P_T G_A G_T(0,0) G_R(0,0)}{L} \qquad (21)$$

The forward solution is repeatedly evaluated at many locations over the 3-dimensional feasibility space to obtain the optimum fit to the N-point RSS data set via application of the objective function, i.e.:

$$f_e(A_0, \varepsilon', \varepsilon'') = \frac{1}{N}\sum_{n=1}^{N}\{|P_n^{meas}|^2 - |P_n^{calc}(A_0, \varepsilon', \varepsilon'', R_D^n)|^2\} \qquad (22)$$

Note, the function of (22) is essentially a 'least squares fit' routine producing the optimal fit between all N measured power points (P_n^{meas}) and the forward solution counterparts (P_n^{calc}) as derived from (20) above. The values of $A_0, \varepsilon', \varepsilon''$ which produce the global or lowest minimum of the objective function is the solution to the optimization or inversion exercise.
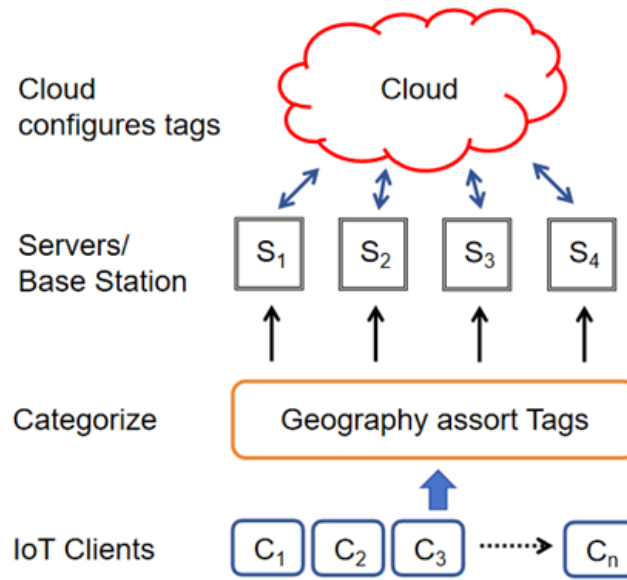
4.3 Geometric Objective Based Federated Learning Algorithm

According to the theory in paper [19], it is impractical to presume that the collected data sets from all sparse learners are drawn from the same distribution (IID) when deploying federated learning systems where distributed learners have diverse environments.

In our problem, we assume that there are n learning nodes deployed in heterogeneous environments (non-IID local data sets). Thus, it is reasonable for nodes to train the model that fits its own statistical pattern. Initially, all nodes are configured with the identically MLSL model assigned with the same parameters with each other. In each iteration, nodes train the model with their locally collected data sets N$_1$, N$_2$, ..., N$_n$ and upload updated models to the server for aggregation. For the traditional IID scenarios, the global weight parameter is computed as the weighted average from the aggregated local weights. However, for non-IID cases, the FedAvg approach can fail to reflect the actual global weight. The diverse patterns

of sub-data sets N_1 through N_n indicate that there is no uniformly joint global model to obtain the best performance for all nodes.

Compared to the learning goal of one empirical path loss model, the model training target for distributed non-IID data sets is to compute the optimized parameter weights for each node rather than a global one for traditional IID data sets. In other words, we divide one federated learning task into several simultaneous ones based on the data set distribution. Whilst inside the cluster, each node is still under the IID pattern and works collaboratively with the FedAvg approach. Here, three individual FL cluster would be distinguished according to the Algorithm 1. Based on the geometric optimization factors, the receiver location can be sorted as LoS, Obstacled-LoS, and Non-LoS the major obstacles are vegetation and terrain block. The three cluster will be denoted as FL1, FL2, and FL3 in section V.

Fig. 4. A flow chart to explain the federated learning structure. Geometric-based tags are added to the signal packet in order to distinguish the FL cluster.

Algorithm 1 Objective based data cluster selection

1: Local sensors collect data packet N_i containing 3-D geometric parameters x, y, z, R_D^n.
2: Edge CPU calculates optimized parameters $P_C^{FF}, P_C^{NF}, \sigma i$.
3: Cluster FLi model, where FLi refers to the selection cluster number.
4: Fetch initial weight parameters $P_C^{FF}, P_C^{NF}, \sigma i, D_{nearfield}$.
5: Set threshold δ (3dB, default) for global weight evaluation.
6: Load N_1.
7: **while** N_i packet's geometric parameter $R_D^n \leq D_{nearfield}$ **do**
8:        **if** $\sigma i \geq \hat{\sigma} + \delta \,\|\, \sigma i \leq -\hat{\sigma} - \delta$ **then**
9:                Calculate N_i packet's power P_C^{FF}, P_C^{NF} and save to $FL2$.
10:               Train equation (20) and (21) locally with dataset $FL2$.
11:               Optimal $f_e(A_0, \varepsilon', \varepsilon'')$.

12:		Create local MLSL model for $FL2$ scenario.
13:	**else**	
14:		Calculate N_i packet's power P_C^{FF}, P_C^{NF} and save to $FL1$.
15:		Train equation (20) and (21) locally with dataset $FL1$.
16:		Optimal $f_e(A_0, \varepsilon', \varepsilon'')$.
17:		Create local MLSL model for $FL1$ scenario.
18:	**end if**	
19: **end while**		
20: **if** N_i packet's geometric parameter $R_D^n > D_{nearfield}$ **then**		
21:	Calculate N_i packet's power P_C^{FF}, P_C^{NF} and save to $FL3$.	
22:	Train equation (20) and (21) locally with dataset $FL3$.	
23:	Optimal $f_e(A_0, \varepsilon', \varepsilon'')$.	
24:	Create local MLSL model for $FL3$ scenario.	
25:	Load the next N_i.	
26: **end if**		
27: For all new packets, run step 6 to step 26 to sort and optimize the models.		

5. Performance Analysis

    In this section, one empirical case study is analyzed in order to prove the performance of the novel method introduced in the paper. The propagation studies form part of a preliminary investigation into the viability of establishing a wireless sensor network (for essential flood detection) in the Colima district of Mexico. For the topographical scenarios in Colima, the two-ray path is a commonly adopted template [26], which usually provides a realistic representation of the channel response for combinations of transmit and receive heights and terrains where both direct line-of-sight (LOS) and secondary ground waves are readily supported. Such models are typically characterized by near-range constructive and destructive interference patterns and an enhanced fourth power roll-off or decay at greater distances. The case is perfectly fitting for the research topic of our method.
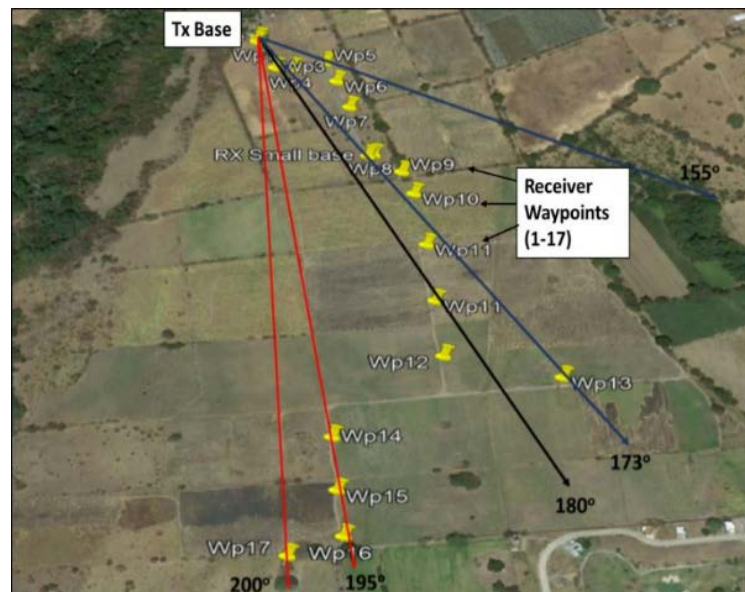
Fig. 5. Aerial view of the Mexican Colima terrain over which the RSS vs Distance, 915 MHz CW, measurements were conducted showing way-point locations 1 to 17 as listed in **Table 3** below.

5.1 Measurement Process and Geometric Objective Calculation

A summary of the link budget parameters for this test configuration is provided in **Table 2**. The way-points shown in **Fig. 5** are coincidental with the RF receiver locations for the required RSS measurements and although a total of 45 were used, the position information of just 17 of these are listed in **Table 3** for brevity. Geometric objectives presented in **Table 3** are calculation according to equation (1)-(8).

Table 2. Channel Sounder Configuration TX / RX Parameters as Used in RSS vs Distance Measurements in **Fig. 5**.

| Parameter	Value	Symbol
Source Modulation	CW	N/A
Source Wavelength	0.328 m	λ
Source Tx Power	10 dBm	P_T
Tx Feeder Loss	6 dB	L_T
Tx Antenna Gain	10 dBi	G_T
Rx Antenna Gain	5 dBi	G_R
Rx Feeder Loss	6 dB	L_R
Rx LNA Gain	20 dB	G_A
Rx LNA Noise Fig.	1.2 dB	G_A
Tx Antenna Height	1.8 m	h_T
Rx Antenna Height	1.8 m	h_R

Table 3. Original 'Spy Glass' Polar \& Cartesian Equivalent Parameters for Measurement Way-points Locations Presented in **Fig. 5**.

Way Point No.	Dist. R_D (m)	Height Rel. to Ref.(m)	Az. (ϕ) (Deg)	El (θ) (Deg)	x_n (m)	y_n (m)	z_n (m)
0	0.0	0.0	0.0	0.0	0.0	0.0	0.0
1	8.7	0.0	34.8	0.0	7.14	0.0	0.0
2	71.6	-2.4	3.3	- 1.9	71.4	-2.4	-2.4
3	87.0	- 1.7	- 12.7	- 1.1	84.9	- 1.7	- 1.7
4	112.1	0.9	-35.0	0.5	91.8	0.7	0.9
5	149.5	0.1	-24.6	0.0	136.0	0.1	0.1
6	202.6	0.0	- 16.3	0.0	194.5	0.0	0
7	303.7	-0.8	-8.9	-0.2	300.0	-0.8	-0.8
8	353.4	-9.9	- 10.9	- 1.6	346.8	-9.7	-9.9
9	402.5	-8.7	-9.2	- 1.2	397.2	-8.6	-8.7
10	498.9	- 10.1	-4.4	- 1.2	497.3	- 10.1	- 10.1
11	600.3	- 15.7	-0.5	- 1.5	600.1	- 15.7	- 15.7
12	698.8	- 19.4	2.2	- 1.6	698.0	- 19.4	- 19.4
13	800.2	- 18.8	-6.7	- 1.3	794.6	- 18.7	- 18.8

| 14 | 801.3 | - 14.8 | 15.1 | - 1.1 | 773.5 | - 14.3 | - 14.8 |
15	892.3	- 16.9	15.5	- 1.1	859.7	- 16.3	- 16.9
16	969.1	-27.4	15.6	- 1.6	933.0	-26.4	-27.4
17	993.2	- 18.7	19.6	- 1.1	935.5	- 17.6	- 18.7

5.2 Optimization Results

According to the geometric factors obtained in **Table 3**, antenna coupling factor can be calculated as well as the specific enhanced 2-ray model for the measurement data. The direct path coupling factor $D_D(\theta, \phi)$ as defined in (14), has been interpolated and plotted in **Fig. 5** as a function of distance R_D along with the corresponding discrete measurement values (denoted by an 'x'). A study of which shows that deviations of up to 4 dB from the maximum boresight coupling factor are in evidence. Note, the plot also shows the variation in Tx azimuthal angle ϕ in interpolated continuous form with distance for reference purposes. Finally, **Fig. 6** displays the measured data normalized to the direct path coupling factor (15), as compared to the original uncompensated data P_R as a function of distance R_D between transmitter and receiver.
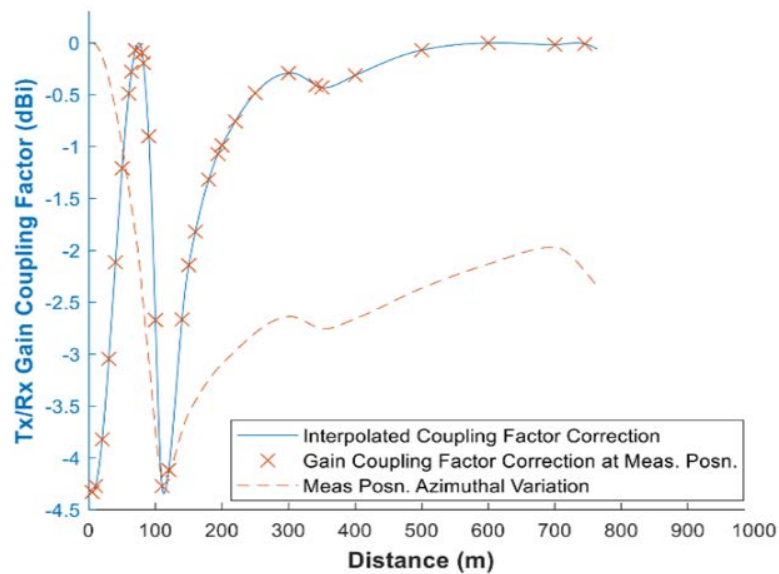
Fig. 6. Coupling Factor $D_D(\theta, \phi)$ as a function of distance ii) same antenna Coupling Factor at the discrete measurement positions in **Fig. 5** iii) variation in transmit / receive antenna azimuth angle (ϕ) from boresight as illustrated in **Fig. 3**.
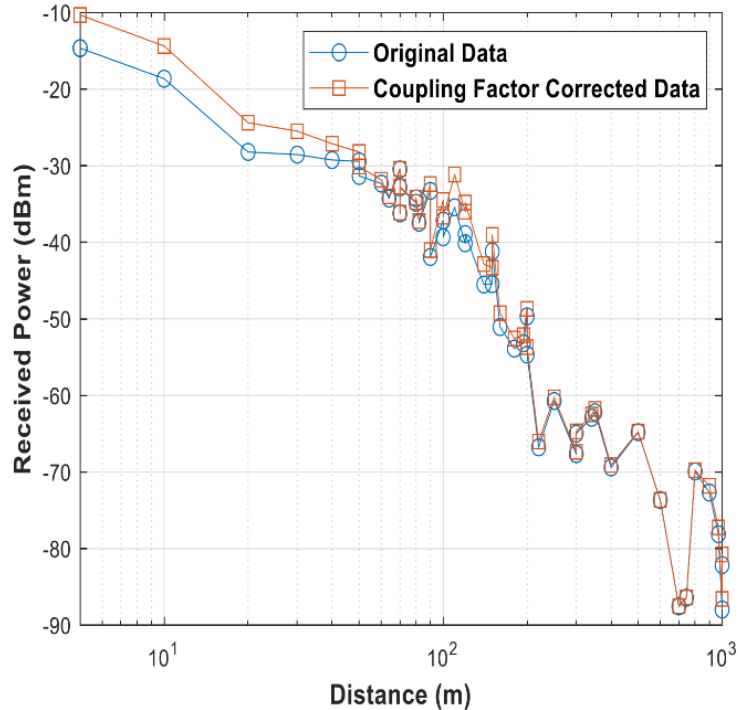
Fig. 7. RSS vs Distance Measurements: Comparison of original measured RSS data and the corrected data derived via normalization to transmit / receive antenna directivity coupling factor $D_D(\theta, \phi)$ shown in **Fig. 6**.

The inversion parameters yielding the global minima, are listed in **Table 4**, whilst the corresponding forward solution values (P_n^{calc}) are plotted as a function of distance R_D along with the measured RSS data in **Fig. 7**. Note, the impressive correlation between the derived ground complex permittivity values (i.e., ε' = 5.36, σ = 0.027 S/m) and those cited in [27]. Even more striking is the close distribution of the measurement points around the two distinct propagation regions, i.e., a 2nd order dependence from 1 to 140 m and a 4th order dependence for 140 m to 1000 m. Also, in evidence are the heavily damped 2-ray path oscillations for ranges < 140 m - verification of the heavy attenuation experienced by the reflected ray due to the high ground conductivity existing in this locality (~ 0.03 S/m).

Table 4. 2-Ray Path Model Parameter Values Optimization: Yielding the Optimal Correlation

Optimization Parameter	Symbol	Value
Tx ERP x Coupling Factor	A_0	1488 mW
Ground Permittivity (Real)	ε'	5.36
Ground Conductivity	$\sigma = (\omega\, \varepsilon''\varepsilon_0)$	0.027 S/m
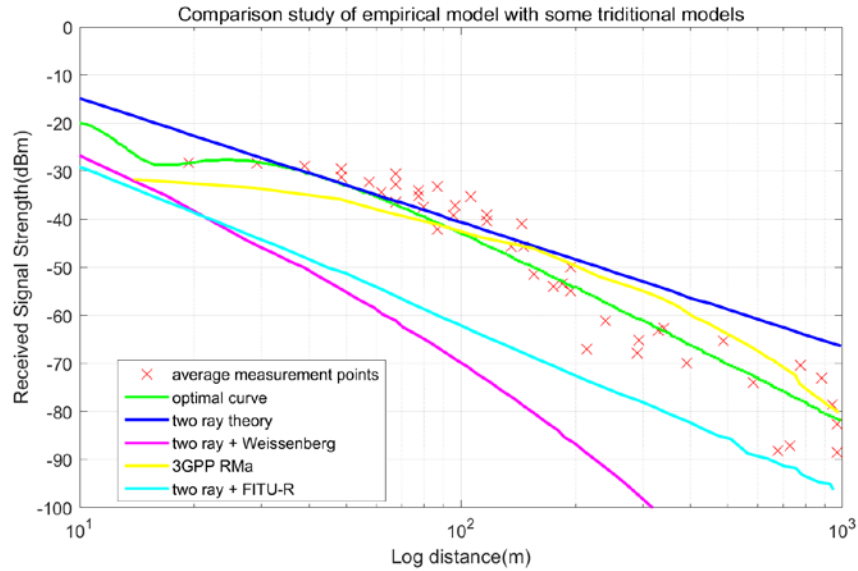
Fig. 8. Results of 2-Ray path model optimisation / inversion analysis and subsequent correlation with Rx Power vs Distance at 915 MHz. Comparison between the two-ray model plus excess loss and the proposed models.

In **Fig. 8**, we also compare the optimal fitting curve with some traditional models. Since the main obstacles are vegetation, we select several vegetation exceed loss model combining with normal two ray model. The application of the Weissenberg model is applied to environments where the ray path is blocked by means of a dense, dry, in-leaf trees forest [28]. FITU-R model estimates the signal loss in an environment with forest, which provide models of signal loss for trees scenario [29]. 3GPP TR 38.901 defines propagation models suitable for 5G NR 0.5-100 GHz based on multiple scenarios, including four categories of scenarios: Uma, UMi, RMa, and InH [30], [31]. The specific scope of Rural macro station application is as follow: Suitable for areas with very sparse distribution of buildings. This type of scenario mainly includes most rural areas and a few underdeveloped township areas. 3GPP-RMa (900MHz) shares the same curve compared to the measurement points. However, exceed vegetation small-scale attenuation is not expressed in the 3GPP model. Our geometric based model fits the measurement points better compared to other selected model combinations. This proves the necessary of short-range close-ground IoT edge device propagation model studies. Furthermore, the trend of optimal curve is different from other vegetation exceed loss model, which means some extra loss may affect together in the environment. However, even our optimal model could not fit most measurement point, when the data size increases. The author believes that the measurement points need to be sorted according to their characteristics. Large amount unrelated data may poison the model's accuracy. Then we implement federated learning cluster selection based on geometric factor to solve the data poison problem.

5.3 Model Correction Using FL Algorithm

From **Fig. 8** we can find that the empirical model considering all the measurement points suffered from the same problem as we mentioned at the beginning. That the optimal curve still could not fit for the most measurement point, especially those with high exceed loss opponent. Here we use the Algorithm 1 mentioned in section IV to distinguish the data. Measurement points would be allocated with LOS (FL1), OLOS (FL2), NLOS (FL3) tags, using 3-D

geometric factors collected by the sensor. By selecting site-specific data, we can obtain accurate geometric based cluster's propagation model. **Fig. 9** describes three clusters optimized propagation model compared to the entirely data empirical model. Each cluster model fits a group of measurement points, further data with the same tag will be trained in the same group. The benefit comes from less standard deviation, higher model accuracy, and less computing time. However, large number reasonable data is needed or the curve may have jitter.
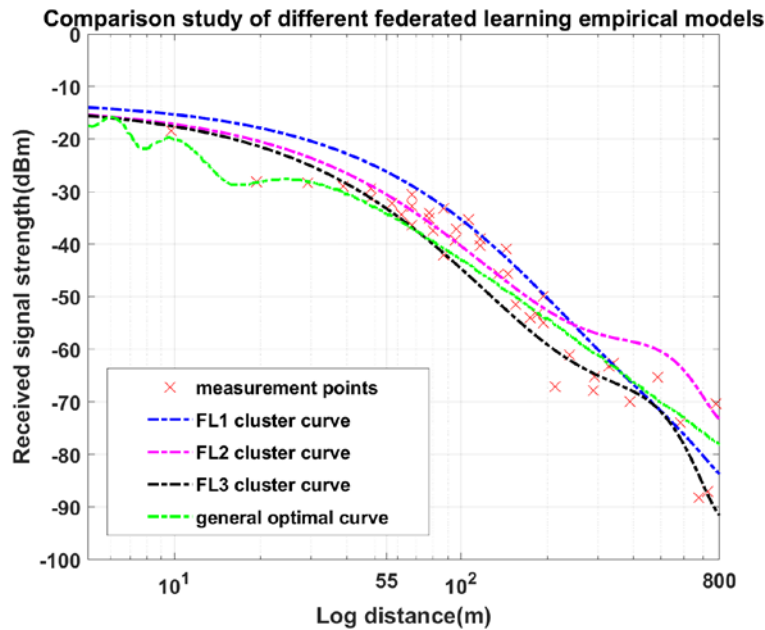

Fig. 9. Optimised propagation model using Algorithm 1 to select new clusters. The three FL clusters: LOS (FL1), OLOS (FL2), NLOS (FL3) are distinguished from the geometric factors counted.

6. Conclusion

In this paper, the novelty of the test conditions contained herein, originated from the necessity to deviate from the straight-line vector between the original test transmit and receiver locations due to man-made & natural obstructions. The RSS vs distance data processing accounted for this anomaly via implementation of a novel 3-D propagation path model incorporating the ground slope and off bore-sight antenna alignments. Subsequent studies of the transmit-receive antenna coupling via complex 3-D geometric analyses, demonstrated that an enhanced two ray path model.

The results of propagation optimization methods in the paper proved undulating terrain in the Colima district of Mexico. Enhanced propagation models are summarized and post-processed to obtain a complex channel transfer function designed to determine the robustness of intended future sensor network links for flood detection.

Further work could entail a direct comparison between measured and modelled RSS data in the above environment, and a comparison of the 2-ray path dispersion model with that provided by software simulations considering wider range frequency for the next generation IoT network.

References

[1] F. Guo, F. R. Yu, H. Zhang, X. Li, H. Ji and V. C. M. Leung, "Enabling Massive IoT Toward 6G: A Comprehensive Survey," *IEEE Internet of Things Journal*, vol.8, no.15, pp.11891-11915, Aug.1, 2021. Article (CrossRef Link)

[2] D. Y. Koh, T. S. Han and J. Zubah, "Electromagnetic Wave Sensor for Proximity Target Detection Under Radio and Radar Coexistence at 2.4-GHz ISM Band," in *Proc. of 2021 IEEE Sensors*, pp.1-4, 2021. Article (CrossRef Link)

[3] H. De Oliveira, M. Kaneko, L. Boukhatem and E. H. Fukuda, "Deep Reinforcement Learning-Aided Optimization of Multi-Interface Allocation for Short-Packet Communications," *IEEE Transactions on Cognitive Communications and Networking*, vol.9, no.3, pp.738-753, Jun. 2023. Article (CrossRef Link)

[4] G. Caso, Ö. Alay, L. De Nardis, A. Brunstrom, M. Neri and M. -G. Di Benedetto, "Empirical Models for NB-IoT Path Loss in an Urban Scenario," *IEEE Internet of Things Journal*, vol.8, no.17, pp.13774-13788, Sep.1, 2021. Article (CrossRef Link)

[5] M. G. Gaitán et al., "Modeling LoRa Communications in Estuaries for IoT Environmental Monitoring Systems," *IEEE Sensors Journal*, vol.22, no.21, pp.21312-21325, Nov.1, 2022. Article (CrossRef Link)

[6] X. Wang, X. Zhang, S. Wang, J. Xiao and X. Tao, "Modeling, Critical Threshold, and Lowest-Cost Patching Strategy of Malware Propagation in Heterogeneous IoT Networks," *IEEE Transactions on Information Forensics and Security*, vol.18, pp.3531-3545, 2023. Article (CrossRef Link)

[7] J. Hejselbæk, J. Ødum Nielsen, W. Fan and G. F. Pedersen, "Empirical Study of Near Ground Propagation in Forest Terrain for Internet-of-Things Type Device-to-Device Communication," *IEEE Access*, vol.6, pp.54052-54063, 2018. Article (CrossRef Link)

[8] R. El Chall, S. Lahoud and M. El Helou, "LoRaWAN Network: Radio Propagation Models and Performance Evaluation in Various Environments in Lebanon," *IEEE Internet of Things Journal*, vol.6, no.2, pp.2366-2378, Apr. 2019. Article (CrossRef Link)

[9] S. Salous, Radio Propagation Measurement and Channel Modelling, Malaysia: John Wiley & Sons, pp.59-61, 2013. Article (CrossRef Link)

[10] M. Nakhkash, Yi Huang and M. T. C. Fang, "Application of the multilevel single-linkage method to one-dimensional electromagnetic inverse scattering problem," *IEEE Transactions on Antennas and Propagation*, vol.47, no.11, pp.1658-1668, Nov. 1999. Article (CrossRef Link)

[11] F. Sattler, S. Wiedemann, K. R. Müller, and W. Samek, "Robust and Communication-Efficient Federated Learning From Non-i.i.d. Data," *IEEE Transactions on Neural Networks and Learning Systems*, vol.31, no.9, pp.3400-3413, Sep. 2020. Article (CrossRef Link)

[12] G. Xu, H. Li, S. Liu, K. Yang and X. Lin, "VerifyNet: Secure and Verifiable Federated Learning," *IEEE Transactions on Information Forensics and Security*, vol.15, pp.911-926, 2020. Article (CrossRef Link)

[13] H. Zhu and Y. Jin, "Multi-Objective Evolutionary Federated Learning," *IEEE Transactions on Neural Networks and Learning Systems*, vol.31, no.4, pp.1310-1322, Apr. 2020. Article (CrossRef Link)

[14] Cai X, Hu Z, Zhao P et al., "A hybrid recommendation system with many-objective evolutionary algorithm," *Expert Systems with Applications*, vol.159, 2020. Article (CrossRef Link)

[15] H. Sun et al., "IRS-Assisted RF-Powered IoT Networks: System Modeling and Performance Analysis," *IEEE Transactions on Communications*, vol.71, no.4, pp.2425-2440, Apr. 2023. Article (CrossRef Link)

[16] T. O. Olasupo and C. E. Otero, "The Impacts of Node Orientation on Radio Propagation Models for Airborne-Deployed Sensor Networks in Large-Scale Tree Vegetation Terrains," *IEEE Transactions on Systems, Man, and Cybernetics: Systems*, vol.50, no.1, pp.256-269, Jan. 2020. Article (CrossRef Link)

[17] P. Pal, R. P. Sharma, S. Tripathi, C. Kumar and D. Ramesh, "Machine Learning Regression for RF Path Loss Estimation Over Grass Vegetation in IoWSN Monitoring Infrastructure," *IEEE Transactions on Industrial Informatics*, vol.18, no.10, pp.6981-6990, Oct. 2022. Article (CrossRef Link)

[18] H. B. McMahan, E. Moore, D. Ramage, S. Hampson, and B. A. y Arcas, "Communication-efficient learning of deep networks from Decentralized data," in *Proc. of the 20th International Conference on Artificial Intelligence and Statistics*, pp.1273-1282, 2017. Article (CrossRef Link)

[19] M. A. Serhani, H. G. Abreha, A. Tariq, M. Hayajneh, Y. Xu and K. Hayawi, "Dynamic Data Sample Selection and Scheduling in Edge Federated Learning," *IEEE Open Journal of the Communications Society*, vol.4, pp.2133-2149, 2023. Article (CrossRef Link)

[20] T. Nishio and R. Yonetani, "Client Selection for Federated Learning with Heterogeneous Resources in Mobile Edge," in *Proc. of ICC 2019 - 2019 IEEE International Conference on Communications (ICC)*, pp.1-7, 2019. Article (CrossRef Link)

[21] Z. Chen, P. Tian, W. Liao and W. Yu, "Zero Knowledge Clustering Based Adversarial Mitigation in Heterogeneous Federated Learning," *IEEE Transactions on Network Science and Engineering*, vol.8, no.2, pp.1070-1083, 2021. Article (CrossRef Link)

[22] X. Huang, Y. Wu, C. Liang, Q. Chen and J. Zhang, "Distance-Aware Hierarchical Federated Learning in Blockchain-Enabled Edge Computing Network," *IEEE Internet of Things Journal*, vol.10, no.21, pp.19163-19176, Nov.1, 2023. Article (CrossRef Link)

[23] T. Li, A. K. Sahu, M. Zaheer, M. Sanjabi, A. Talwalkar, and V. Smith, "Federated Optimization in Heterogeneous Networks," in *Proc. of Machine Learning and Systems 2 (MLSys 2020)*, 2020. Article (CrossRef Link)

[24] C. A. Balanis, Antenna Theory Analysis & Design, 4nd ed. New York, NY, USA: Wiley, pp.650-653, 2016. Article (CrossRef Link)

[25] M. Nakhkash, Yi Huang and M. T. C. Fang, "Application of the multilevel single-linkage method to one-dimensional electromagnetic inverse scattering problem," *IEEE Transactions on Antennas and Propagation*, vol.47, no.11, pp.1658-1668, Nov. 1999. Article (CrossRef Link)

[26] Flood Prediction using real time sensing Emergency Water Information Networks over mobile phone networks and WiFi (EWIN). UK Research and Innovation. [Online]. Available: https://gow.epsrc.ukri.org

[27] C. Sommer and F. Dressler, "Using the Right Two-Ray Model? A Measurement based Evaluation of PHY Models in VANETs," in *Proc. of 17th ACM MobiCom*, pp.1-3, 2011. Article(CrossRefLink)

[28] M. A. Weissberger, "An initial critical summary of models for predicting the attenuation of radio waves by trees," Defense Technical Information Center, Fort Belvoir, VA, Tech. Rep. ESD-TR-81-101, Jul. 1982. Article (CrossRef Link)

[29] M. O. Al-Nuaimi and R. B. L. Stephens, "Measurements and prediction model optimisation for signal attenuation in vegetation media at centimetre wave frequencies," *IEE Proceedings - Microwaves*, *Antennas and Propagation,* vol.145, no.3, pp.201-206, Jun. 1998. Article (CrossRef Link)

[30] Y. Wang, R. Zhang, B. Li, X. Tang and D. Wang, "Angular Spread Analysis and Modeling of UAV Air-to-Ground Channels at 3.5 GHz," in *Proc. of 2019 11th International Conference on Wireless Communications and Signal Processing (WCSP)*, pp. 1-5, 2019. Article (CrossRef Link)

[31] G. R. MacCartney and T. S. Rappaport, "Rural Macrocell Path Loss Models for Millimeter Wave Wireless Communications," *IEEE Journal on Selected Areas in Communications*, vol.35, no.7, pp.1663-1677, Jul. 2017. Article (CrossRef Link)

Yu Geng received the B.S. degree in communication engineering from Dalian Maritime University, Dalian, China in 2015, the M.S. degree in information communication engineering from University of Leicester, Leicester, UK in 2017, and Ph.D. degrees in communication engineering from Loughborough University, Loughborough, UK, in 2022.

He became a collaborating post-doctor with the National Mobile Communications Research Laboratory, Southeast University and China Information Consulting \& Designing Institute (CICDI) CO., LTD. in 2023. He has authored or co-authored about 10 papers. His research interests include IoT propagation model, wireless sensor networks, and IoT resource allocations.

He was the recipient of Outstanding post-doctor Award from Jiangsu Province in 2023.

Tiecheng Song (Member, IEEE) received the B.S. degree in radio technology, the M.S. degree and Ph.D. degrees in communication and information system from Southeast University, Nanjing, China, in 1989, 1992, and 2006 respectively.

He became an Associate Professor and a Professor with the National Mobile Communications Research Laboratory, Southeast University in 2000 and 2005 respectively. He has authored or co-authored five books and more than 100 papers. He is the main inventor of over 20 patents in China. His research interests include cognitive radio, wireless sensor networks, and vehicle networks.

He was the recipient of four times of the Science and Technology Award from Jiangsu Province.

Qiang Wang received the Ph.D. degree in communication and information system engineering from Nanjing University of Science and Technology, Nanjing, China, in 2002.

He became 5G technology Technical Director of China Information Consulting \& Designing Institute (CICDI) CO., LTD. He is also a Senior Expert of China Telecom Group. He has pressed 4 books and authored over 20 papers. He has long been engaged in research on cutting-edge mobile communication technologies, focusing on wireless network planning, design, and optimization.
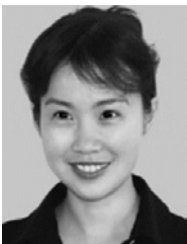
Xiaoqin Song received the Ph.D. degree in communication engineering from Southeast University, Nanjing, China, in 2008.

She joined the College of Electronic and Information Engineering, Nanjing University of Aeronautics and Astronautics, China, in 2008, where she is currently an Associate Professor. She authored more than 50 journal articles and conference papers. She holds more than 20 granted patents. Her current research interests include cooperation communication and wireless networks.